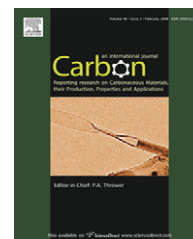


available at www.sciencedirect.comjournal homepage: www.elsevier.com/locate/carbon

Magnetic properties of carbon nano-particles produced by a pulsed arc submerged in ethanol

N. Parkansky^{a,*}, B. Alterkop^a, R.L. Boxman^a, G. Leitush^b, O. Berkh^c, Z. Barkay^d, Yu. Rosenberg^d, N. Eliaz^e

^aElectrical Discharge and Plasma Laboratory, Tel Aviv University, P.O. Box 39040, Tel Aviv 69978, Israel

^bDepartment of Chemical Research Support, Weizmann Institute of Science, Rehovot 76100, Israel

^cSchool of Electrical Engineering, Tel Aviv University, P.O. Box 39040, Tel Aviv 69978, Israel

^dWolfson Applied Materials Research Center, Tel Aviv University, P.O. Box 39040, Tel Aviv 69978, Israel

^eSchool of Mechanical Engineering, Tel Aviv University, P.O. Box 39040, Tel Aviv 69978, Israel

ARTICLE INFO

Article history:

Received 14 February 2007

Accepted 6 November 2007

Available online 21 November 2007

ABSTRACT

Carbon powder was produced by a pulsed arc ignited between two carbon electrodes submerged in ethanol, and was comprised of both micro- and nano-particles. The measured magnetic properties of the mixed “raw” powder at 20 and 300 K were: saturation magnetization $M_s \sim 0.90\text{--}0.93$ emu/g, residual magnetization $M_r = 0.022$ and 0.018 emu/g, and coercive force $H_c = 11$ and 8 Oe, respectively. The data lead to conclusion that the powder consisted of ferromagnetic particles with a critical temperature much higher than 300 K. Magnetic particles in solution were separated by means of bio-ferrography. It was found that the magnetically separated particles included chains of $\sim 30\text{--}50$ nm diameter spheres, and nanotubes and nanorods with lengths of $50\text{--}250$ nm and diameters of $20\text{--}30$ nm. In contrast, the residual particles which passed through the bio-ferrograph consisted of $1\ \mu\text{m}$ and larger micro-particles, and nano-particles without any definite shape.

© 2007 Elsevier Ltd. All rights reserved.

1. Introduction

The possibility of macroscopic magnetic ordering in carbon particles is interesting because of their importance for physics, chemistry and materials science. There may be applications for them in engineering, and, because they are a unique biocompatible magnetic material, in medicine and biology as well [1,2]. Some experiments demonstrated the existence of weak ferromagnetic-like magnetization loops in highly-oriented pyrolytic graphite (HOPG) [3,4] and paramagnetism of a novel carbon nano-foam [5]. There have been theoretical and experimental demonstrations that ferromagnetism can exist in pure carbon [6–11], while other authors refute this possibility [12]. Possibly the coexistence

of sp^3 and sp^2 bonds [1] and defects in graphite structures, such as pores, planar edges and topological defects, induce the observed magnetic properties. Thus, the magnetic properties may depend on the particle production method, since it influences defect production.

Recently, a novel method to produce carbon micro- and nano-particles using a pulsed arc submerged in liquid was developed [13,14]. A plasma bubble is formed, comprised of some combination of material evaporated and partially ionized from the electrodes and the liquid, and in some cases liquid droplets of the electrode material are also produced. Solid particles form when these liquid electrode droplets contact the surrounding liquid and when the materials in the bubble condense, either on contacting the surrounding liquid

* Corresponding author. Fax: +972 3 641 0189.

E-mail address: naump@eng.tau.ac.il (N. Parkansky).

0008-6223/\$ - see front matter © 2007 Elsevier Ltd. All rights reserved.

doi:10.1016/j.carbon.2007.11.008

interface, or as the bubble collapses at the end of the arc pulse [14]. While the morphology of carbon particles produced in submerged arcs has been studied, their magnetic properties have not. The objective of this work was to characterize carbon-particles produced by a pulsed submerged arc, and in particular to measure their magnetic properties.

2. Experimental details

Carbon-particles were produced by a pulsed arc, ignited between two 4 mm diam, 99.99% C graphite electrodes with a gap of 0.35 mm between them, submerged in 200 mL of analytical (99.8%) ethanol contained in a glass beaker. Pulses were generated by a Blumlein transmission line circuit. After each pulse discharge, the transmission lines were charged again, and discharges with $\sim 1 \mu\text{s}$ duration occurred repetitively during free-running operation at a pulse repetition rate of $\sim 1 \text{ kHz}$. The breakdown voltage in ethanol was 12 kV, and the peak current was 250 A.

Powder samples were obtained by extracting liquid with suspended particles from the treatment vessel, transferring it to a glass microscope slide and allowing the liquid to evaporate. Some extracted liquid samples were transferred to a 200 mesh copper grid coated with a carbon film, evaporated, and then examined in a Philips Tecnai F20 transmission electron microscope (TEM). Such samples, i.e. without magnetic separation (to be described below), will be subsequently referred to as “raw” powder. The composition of the electrodes and produced powders were examined by X-ray photoelectron spectroscopy (XPS), with a scanning XPS multi-technique system (PHI 5600, USA). In other tests, the raw powder was examined by X-ray diffraction (XRD) using $\text{CuK}\alpha$ radiation in a θ - θ powder diffractometer equipped with a liquid nitrogen cooled Ge solid-state detector. Magnetic properties of the raw powder were studied using a Quantum Design SQUID MPMS₂ field-shielded magnetometer. The DC (direct current) magnetic moment was measured on 30.1 mg, which was placed in a gelatin capsule held by polyethylene straw. The absolute value of the magnetic signal of the sample holder did not exceed $7 \times 10^{-7} \text{ emu}$ at 200 Oe over the whole temperature range which was applied. The magnetic susceptibility was measured in the ZFC (zero field

cooled) and FC (field cooled) modes at 100 Oe while heating the sample in temperature steps of $\sim 2 \text{ K}$ from 2 to 300 K after cooling it from 300 K. Standard deviations do not exceed of 0.04% (mean std 0.005%) for temperature dependence, and 1% (mean std 0.04%) for field dependence.

Magnetic particles were separated from the non-magnetic particles contained in suspensions by using a Bio-Ferrograph 2100 (Guilfoyle, Inc.). This instrument flowed liquid with suspended particles past a magnetic field that had maximum field strength across an interpolar gap. There magnetically susceptible particles were captured on a microscope slide [15], while the residual liquid, with non-magnetic particles, was collected in disposable syringes. The residual liquid was later transferred onto microscope slides and evaporated, and the slide was microscopically inspected for residual particles. Samples collected by the magnetic field will be subsequently referred to as “magnetically separated”, while samples extracted from the syringes will be referred to as “residual”. Both the “magnetically separated” and “residual” particles were examined in a Quanta 200 FEG environmental scanning electron microscope (FEG-ESEM).

3. Results and discussion

XPS results showed that the raw powder contained carbon, and no metallic elements were detected, indicating that any possible metal contamination was less than 0.01%. The XRD spectrum of the raw powder and that of the electrode material showed only graphite lines.

Typical HRTEM images of micro- and nano-particles contained in the raw carbon powder are presented in Figs. 1a and b, respectively. The particles had spherical, cylindrical and indefinite shapes.

Figs. 2a–c show high-magnification HRTEM micrographs of some nano-particles in the raw samples. Spheroids, nanotubes and nanorods are observed, comprised of layers with an inter-layer spacing of 0.35 nm, close to that of graphite. There were also other nano-particles whose structure, if any, could not be discerned.

Fig. 3 shows DC magnetic moment of the raw powder as a function of magnetic field at $T = 20 \text{ K}$ and 300 K, obtained

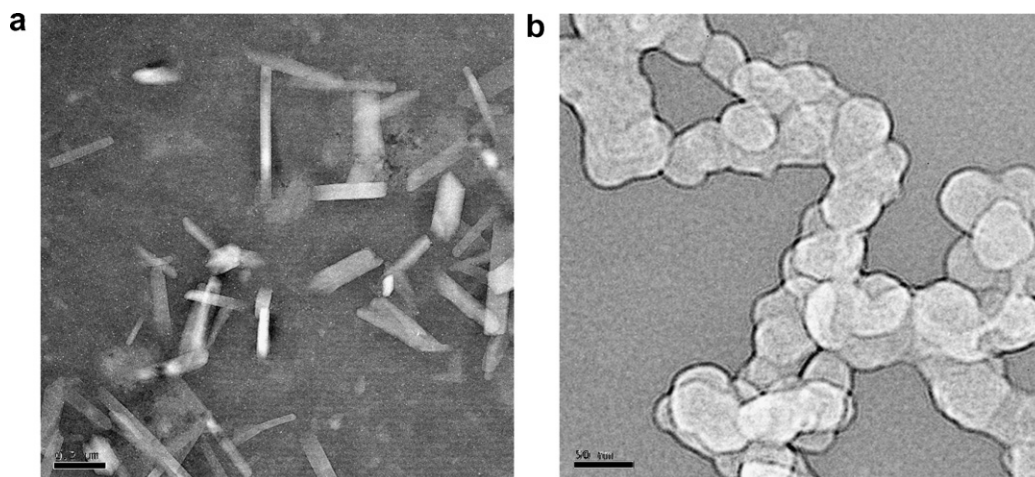


Fig. 1 – HRTEM images of typical forms of the produced micro- and nano-particles in the raw powder.

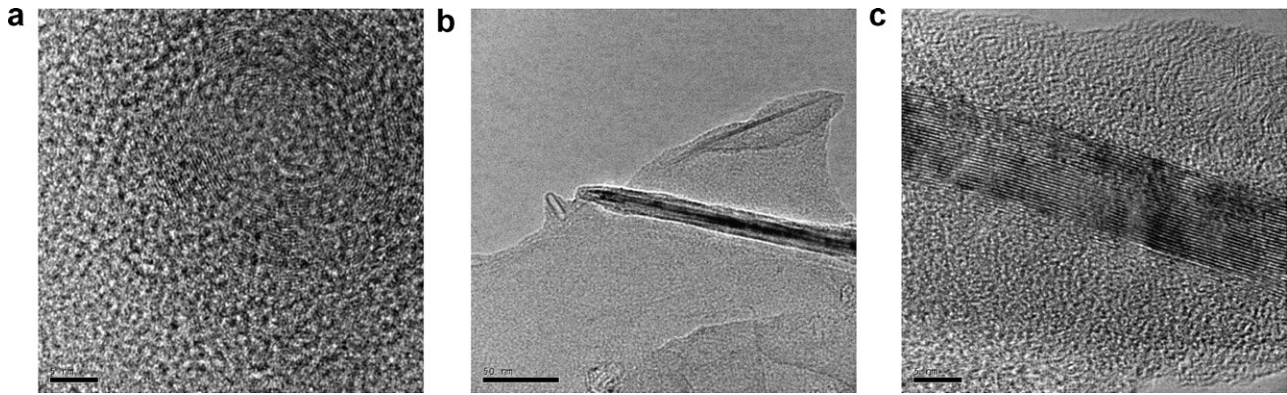


Fig. 2 – HRTEM micrographs of the obtained spheroid (a), nanotube (b), and nanorod (c).

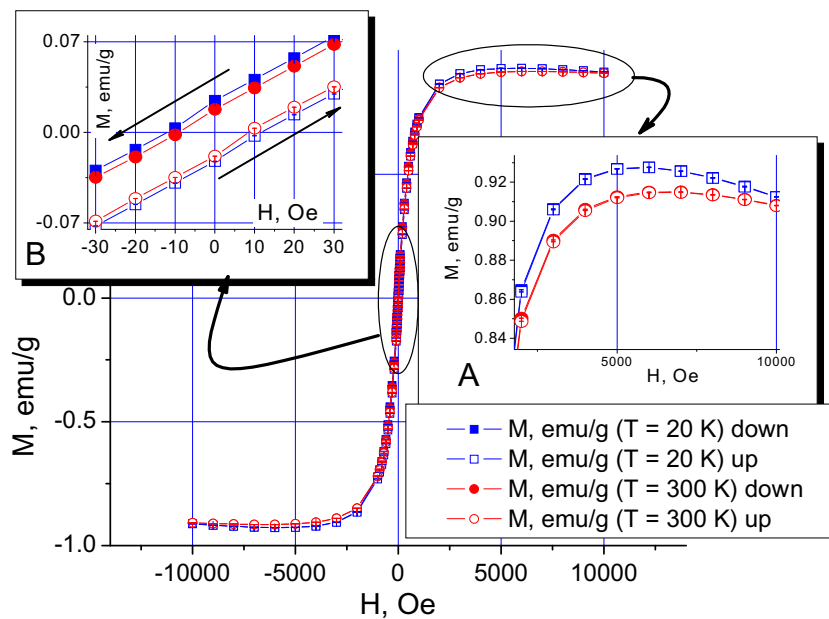


Fig. 3 – Dependence of DC magnetic moment of the raw powder on magnetic field at $T = 20$ K and 300 K. The magnetic field was decreased from 10,000 Oe to $-10,000$ Oe and then increased back. Insets: (A) The dependencies at fields $H > 2000$ Oe; (B) Low-field parts of the curves.

when the magnetic field was decreased from 10,000 Oe to $-10,000$ Oe and then increased back. The demagnetization curves show that the saturation magnetic moment (M_s) was about 0.90–0.93 emu/g (Fig. 3A), the coercive force (H_c) was 11 and 8 Oe, and the residual magnetization (M_r) was 0.022 and 0.018 emu/g, respectively (Fig. 3B). It is seen that the magnetic moment decreased at fields $H > 6000$ Oe. It is a result of a diamagnetic contribution at the fields, more than the saturation field strength (Fig. 3A). This diamagnetic contribution at room temperature can be estimated as $\chi_D = -5.6 \times 10^{-6}$ emu/cm³ (-2.14×10^{-6} emu/g). It can be explained as orbital diamagnetism of internal atoms of carbon nano-particles (room temperature magnetic susceptibility of graphite is $\chi_D = -6 \times 10^{-6}$ emu/cm³). Fig. 4 shows the ZFC and FC temperature dependences of DC magnetic mass susceptibilities measured at a field $H = 100$ Oe. The presented results suggest that the C nano-particle powder has long-range magnetic order and a

critical temperature T_c that is much higher than 300 K. The ferromagnetic-like behavior of the carbon nano-particles is clearly observed in Figs. 3 and 4. It is possible that the observed small irreversibility between ZFC and FC dependencies arises from the fact that a small part of the powder consists of individual domains and behaves superparamagnetically.

In principle, it is possible that the observed weak magnetization originate, from strongly magnetic impurities. However, we estimated the required impurity concentration and compared it with the limit of impurity detection in the raw samples. Considering for example Fe contamination, with a magnetization of 220 A m²/kg [9], we obtained that the iron impurity concentration would need to be ~ 0.004 (0.4 wt%) to produce the observed saturation magnetic moment of ~ 0.9 A m²/kg. This contamination level is more than an order of magnitude greater than the upper limit of the impurity

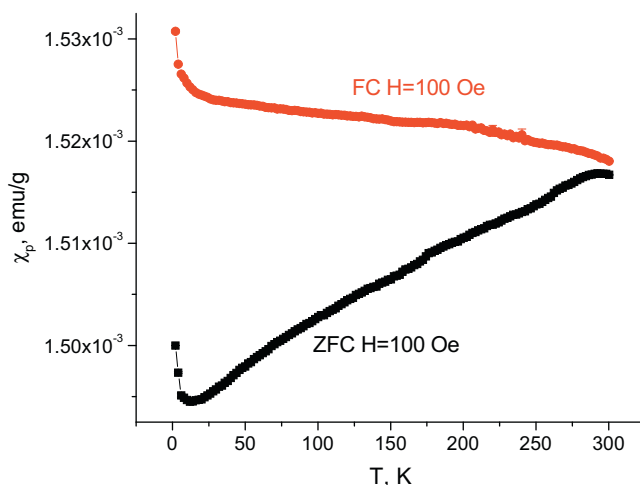


Fig. 4 – ZFC and FC temperature dependencies of DC magnetic mass susceptibilities measured at a field $H = 100$ Oe.

concentration (i.e. <0.01%) in our raw powder. Therefore, the observed magnetic properties cannot be explained by ferromagnetic impurities.

The origin of the carbon particle magnetism is yet not well understood – different speculations are considered as possible reasons of the phenomenon. Our results do not provide information which can explain the origin of magnetism. Irradiation by fast particles, dangling bonds and intrinsic defects like vacancies or interstitial atoms on the particle surface and their interaction with different adatoms were considered to be responsible for magnetic properties [7,16–18]. All these phenomena might possibly occur in our experiment. For example, the produced particles may be irradiated by fast ions (e.g. H^+) created as a result of the ethanol decomposition and accelerated at the applied electrical potential of 12 kV. Using the average measured particle diameter of ~ 40 nm and the saturation magnetization of 0.9 emu/g, we obtain a magnetic moment of $\sim 0.004 \mu B$ per carbon atom, or $\sim 0.04 \mu B$ per carbon atom on the particle surface. The last rough evaluation exceeded by more than an order of magnitude the lim-

its of the interval estimated by Ohldag et al. [10] for the magnetic ring area of proton irradiated metal-free carbon. Following the procedure of Hohne et al. [11] and taking into account the observed weak temperature dependences (Fig. 4), we assume that the calculated high value of the magnetic moment is determined by two contributions: a temperature independent contribution (it can be, in general, a result of the competition of Pauli paramagnetic and Landau diamagnetic terms) and a temperature dependent contribution which mostly arises from unpaired electrons localized on dangling bonds on the carbon nano-particle surfaces.

To determine what kind of particles are responsible for the magnetic behavior, the magnetic particles were separated from the non-magnetic particles contained in the raw suspension by bio-ferrography [19]. Typical ESEM secondary electron images of the magnetically separated particles are shown in Figs. 5a and b.

Two types of nano-particles are clearly identified: agglomerates of ~ 30 – 50 nm diameter spheres (Fig. 5a), and nanotubes and nanorods with length, of 50–250 nm and diameters of 20–30 nm (Fig. 5b). These particles are similar to those observed by HRTEM in the raw powder (Figs. 1a and b). Not only is this similarity important with respect to verification of results by different analytical techniques (which is usually recommended in TEM work, for example), it also demonstrates the high sensitivity and applicability of bio-ferrography in isolating inherently magnetic materials, or magnetized materials, in general. The original shape of the particles is preserved, and even very small particles, on the nano-scale, can be captured from small-volume samples (as small as $1 \mu L$). To the best of the authors' knowledge, this is the first time where the applicability of bio-ferrography in isolation of nano-particles has been demonstrated in the literature. Fig. 6 shows ESEM images of the “residual” particles that passed through the magnetic field of the bio-ferrograph to the disposable syringes. These particles include both micro-particles with characteristic dimension of $1 \mu m$ and larger (i.e. much larger than the “magnetically separated” particles) and nano-particles without well-defined shape. Thus, apparently only the spherical nano-particle chains and cylindrical nanotubes and nanorods have magnetic properties.

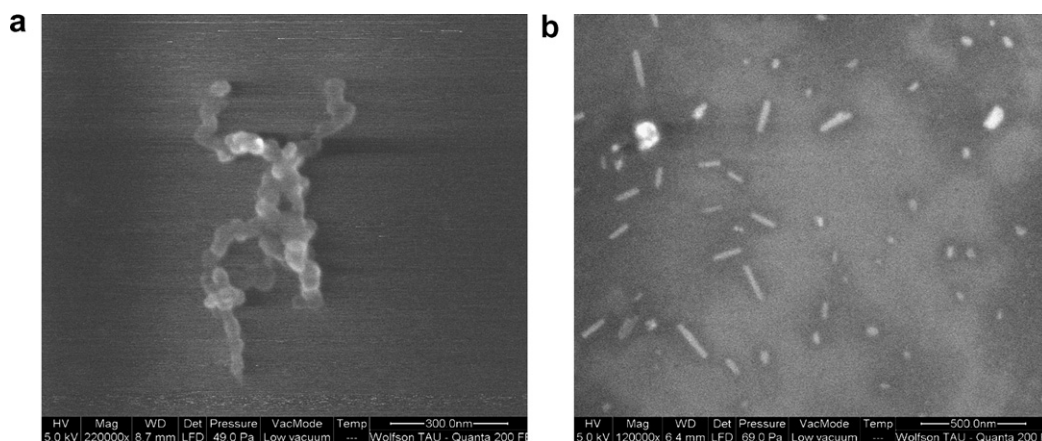


Fig. 5 – ESEM SE images of magnetically separated spherical (a) and rod (b) carbon nano-particles that were captured on glass slides by bio-ferrography.

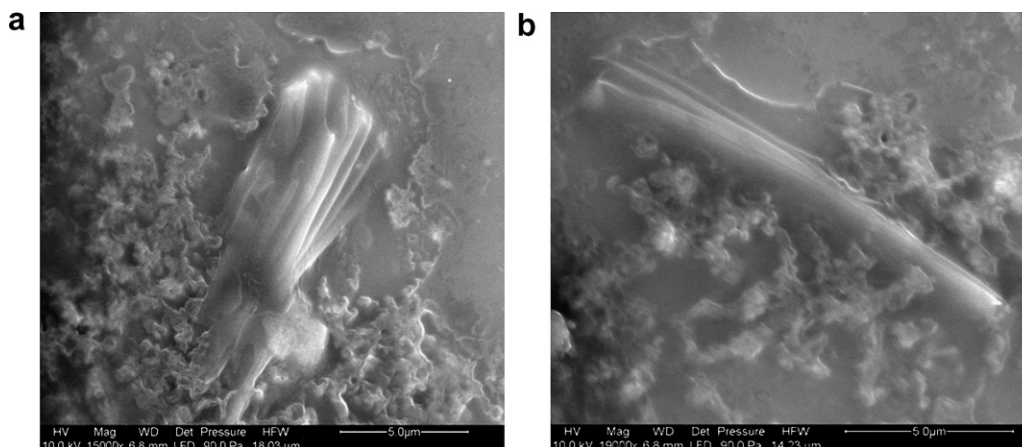


Fig. 6 – “Residual” particles obtained in processed ethanol after magnetic separation.

4. Conclusions

- (1) Carbon powder comprised of nano- and micro-particles was produced by a pulsed arc submerged in ethanol.
- (2) Magnetic particles in solution were separated by means of bio-ferrography, showing that bio-ferrography is effective in capturing nano-particles while preserving their original shape.
- (3) The micro-particles were non-magnetic, while the nano-particles exhibited magnetic behavior. The magnetic properties of the mixed “raw” powder at 20 and 300 K were: $M_s \sim 0.90\text{--}0.93$ emu/g, $M_r = 0.022$ and 0.018 emu/g, and $H_c = 11$ and 8 Oe, respectively. The powder consisted of nano-particles demonstrates a ferromagnetic behavior with a critical temperature much higher than 300 K.

Acknowledgement

The authors gratefully acknowledge collaboration with Metal-Tech Ltd.

Appendix A. Supplementary data

Supplementary data associated with this article can be found, in the online version, at doi:10.1016/j.carbon.2007.11.008.

REFERENCES

- [1] Makarova TL. Magnetic properties of carbon structures. *Semiconductors* 2004;38(6):615–38.
- [2] Pardo H, Faccio R, Araújo-Moreira FM, de Lima OF, Mombrú AW. Synthesis and characterization of stable room temperature bulk ferromagnetic graphite. *Carbon* 2006;44(3):565–9.
- [3] Kopelevich Y, Esquinazi P, Torres JHS, Moehlecke S. Ferromagnetic and superconducting-like behavior of graphite. *J Low Temp Phys* 2000;119(5–6):691–702.
- [4] Esquinazi P, Setzer A, Höhne R, Semmelhack C, Kopelevich Y, Spemann D. Ferromagnetism in oriented graphite samples. *Phys Rev B* 2002;66(2):244291–2442910.
- [5] Rode AV, Gamaly EG, Christy AG, Fitz Gerald JG, Hyde ST, Elliman RG. Unconventional magnetism in all-carbon nanofoam. *Phys Rev B* 2004;70(5):0544071–9.
- [6] Esquinazi P, Spemann D, Höhne R, Setzer A, Han KH, Butz T. Induced magnetic ordering by proton irradiation in graphite. *Phys Rev Lett* 2003;91(22):2272011–4.
- [7] Kusakabe K, Maruyama M. Magnetic nanographite. *Phys Rev B* 2003;67(9):0924061–4.
- [8] Han KH, Spemann D, Esquinazi P, Höhne R, Riede V, Butz T. Ferromagnetic spots in graphite produced by proton irradiation. *Adv Mater* 2003;15(20):1719–22.
- [9] Mombrú AW, Pardo H, Faccio R, de Lima OF, Lanfredi AJC, Cardoso CA. Multilevel ferromagnetic behavior of stable room temperature bulk magnetic graphite. *Phys Rev B* 2005;71:100404(R)1–4.
- [10] Ohldag H, Tylliszczak T, Hohne R, Spemann D, Esquinazi P, Ungureanu M, et al. π -electron ferromagnetism in metal-free carbon probed by soft X-ray dichroism. *Phys Rev Lett* 2007;98:187204.
- [11] Hohne R, Han K-H, Esquinazi P, Setzer A, Semmelhack H, Spemann D, et al. Magnetism of pure, disordered carbon films prepared by pulsed laser deposition. *J Magn Magn Mater* 2004;272–276:E839.
- [12] Coey M, Sanvito S. The magnetism of carbon. *Phys World* 2004:33–7. November.
- [13] Parkansky N, Boxman RL. Production of nanoparticles and microparticles. U.S. Patent Application 10/615,141.
- [14] Parkansky N, Alterkop B, Boxman RL, Goldsmith S, Barkay Z, Lereah Y. Pulsed discharge production of nano- and microparticles in ethanol and their characterization. *Powder Technol* 2005;150(1):36–41.
- [15] Seifert WW, Westcott VC, Desjardins JB. Flow unit for ferrographic analysis, U.S. Patent No. 5,714,059, 1998.
- [16] Kim Y-H, Choi J, Chang KJ. Defective fullerenes and nanotubes as molecular An magnets: *ab initio* study. *Phys Rev B* 2003;68:125420.
- [17] Banhart F. Irradiation effects in carbon nanostructures. *Rep Prog Phys* 1999;62:1181–221.
- [18] Lehtinen PO, Foster AS, Ayuela A, Krasheninnikov A, Nordlund K, Nieminen RM. Magnetic properties and diffusion of adatoms on a graphene sheet. *Phys Rev Lett* 2003;91:017202.
- [19] Ishay JS, Barkay Z, Eliaz N, Plotkin M, Volynchick S, Bergman DJ. Gravity Orientation in Social Wasp Comb Cells (Vespinae) and the Possible Role of Embedded Minerals. *Naturwissenschaften*, doi:10.1007/s00114-007-0334-z.